The tropical Madden-Julian oscillation and the global wind oscillation

Klaus Weickmann

NOAA/ESRL/Physical Sciences Division, Boulder, Colorado

Edward Berry

NOAA/National Weather Service, Dodge City, Kansas

Monthly Weather Review

Revised

October 3, 2008

Corresponding author: Klaus Weickmann

NOAA/ESRL

Physical Sciences Division, R/PSD1

325 Broadway

Boulder, CO 80305-3337

Klaus.Weickmann@noaa.gov

Abstract

The global wind oscillation (GWO) is a subseasonal phenomenon encompassing the tropical Madden-Julian Oscillation (MJO) and mid-latitude processes like meridional momentum transports and mountain torques. A phase space is defined for the GWO following the approach of Wheeler and Hendon (2004) for the MJO. In contrast to the oscillatory behavior of the MJO, two red noise processes define the GWO. The red noise spectra have variance at periods that bracket 30-60 or 30-80 days, which are bands used to define the MJO. The correlation between the MJO and GWO is ~0.5 and cross-spectra show well-defined, coherent phase relations in similar frequency bands. However, considerable independent variance exists in the GWO. A basic dynamical distinction occurs in the direction of mid-latitude wave energy dispersion, being predominantly meridional during a MJO and zonal during the GWO. This is primarily a winter season feature centered over the Pacific Ocean. A case study during April-May 2007 focuses on the GWO and two ~30 day duration orbits with extreme anomalies in GWO phase space. The MJO phase space projections for the same time were irregular and, it is argued, partially driven by mountain torques and meridional transports. The case study reveals multiple physical processes and time scales act to create slowly evolving planetary-scale circulation and tropical convection anomalies.

1. Introduction

Subseasonal, 10-90 day events in the atmosphere's circulation evolve in the frequency band that connects synoptic weather variations and interannual climate behavior. These atmospheric fluctuations influence the statistics of extreme weather events and can initiate rapid changes in the interannual climate. Such abrupt or extreme developments are at the frontier of weather and climate prediction. Moreover, interactions within this band between internal (e.g., jet stream) atmospheric dynamics and 'external' boundary forcing (e.g., sea surface temperature) influence the evolution of the coupled ocean-atmosphere system. Understanding the time and space scales of the band, and its interaction with adjacent time bands, is a scientific challenge with applications to global weather-climate modeling and extended range prediction.

The tropical Madden-Julian Oscillation (MJO; Madden and Julian, 1972) and the extratropical teleconnection patterns (Wallace and Gutzler, 1981) are phenomena that bridge weather and climate. They have inherent lifetimes between 10-90 days and are linked with variations in the global or near-global circulation. Additional global teleconnection patterns have been proposed by Branstator (2002) and Weickmann and Berry (2007; hereafter WB). Such phenomena can be used to monitor the time-evolving large-scale atmospheric circulation, the pattern of large-scale tropical convection and the ongoing influence of coherent tropical-extratropical interactions.

Atmospheric angular momentum (AAM) provides a convenient framework (Peixoto and Oort, 1992) to track these subseasonal weather-climate phenomena, and is a starting point for monitoring their regional impacts. Nearly 30 years ago Langley et al. (1981) documented the presence of ~50 day variations in length of day and global AAM. Anderson and Rosen (1983) linked these variations to the MJO and analyzed a coherent poleward and downward propagation of zonal mean zonal wind anomalies. Global AAM anomalies peaked as the zonal mean zonal wind anomalies moved into the subtropics. The AAM link to the MJO was further explored by Madden (1987) who showed global AAM is largest when MJO convection anomalies are weakening near the Dateline.

Madden (1987, 1988) proposed that frictional torque anomalies over the Pacific Ocean basin to the east of convection anomalies were responsible for the exchange of angular momentum between the atmosphere and the earth. Although the mountain torque appeared to be small, subsequent investigations (Weickmann et al., 1992; Madden and Speth, 1995; Hendon, 1995; Weickmann et al., 1997 hereafter WKS) proposed approximately equal roles for the friction and mountain torque in forcing the global AAM changes.

In contrast to the focus on the MJO, several studies (Ghil and Childress, 1987; Dickey, Ghil and Marcus, 1991; Ghil and Robertson, 2002) argued for a separate ~40 day AAM oscillation in the extratropical atmosphere forced primarily by the mountains and their interaction with zonally asymmetric circulation anomalies (Marcus et al., 1996). Oscillatory forcing by the extratropical mountain torque in the 20-30 day band was also proposed (e.g., Lott et al., 2004; Lott et al., 2005). The idea of independent intraseasonal global AAM oscillations, one forced by mountain torques in the extratropics and the other by convection in the tropics was postulated and the former process studied by Marcus et al., (1994) and Jin and Ghil (1990).

Weickmann, et al, 2000 (hereafter WRP) also argued for a separate mode of subseasonal global AAM variation but rather than a nonlinear oscillation they assumed it was a linear stochastically forced mode (Sardeshmukh and Sura, 2008). The underlying physics and time scale was linked to the atmosphere's attempt to maintain global AAM balance in the presence of large or clustered mountain torque events. Composites show atmospheric wave patterns over the major mountain ranges that produce either easterly or westerly wind anomalies over the topography. These patterns disperse downstream and can flux AAM meridionally. A zonal mean analysis confirms impulsive momentum fluxes, especially across ~30-40N, play a dual role of exciting the mountain torque and transporting the resulting momentum from mountainous source regions to frictional sink regions via mid-latitude eddies. A characteristic feature of this adjustment process is a quadrature relation in global time series of the friction and mountain torque with the frictional torque leading. Coherent variations of the circulation that accompany the

process include the well-known PNA teleconnection pattern and zonal index variations (Weickmann, 2003 hereafter W03).

The slow time scale governing the global evolution of this separate extratropical mode is assumed to be the ~6-day decay time of the global frictional torque (WRP). A red noise spectrum (Wilks, 1995) with a 6-day decay time would show broadband variance centered at 2π x 6 days= ~40 days, and thereby the frictional torque would force AAM variations with power concentrated around 40 days. The MJO produces variance in a similar frequency band and the interaction between it and the mid-latitude-dominated frictional red noise process is viewed as a prototype for tropical-extratropical interaction.

Using AAM as a framework, WB advocated a global to regional approach to monitoring short term climate variations and evaluating subseasonal predictions by GCMs. This includes evaluation of zonal mean anomalies and the interaction of multiple time/space scale physical processes within a dynamical weather-climate linkage framework. Global indices provide the big picture on the atmosphere's state and are linked to the zonal mean and then regional behavior of the circulation, including teleconnection patterns. WB chose three indices to represent multiple subseasonal time scales. Daily indices of the Madden-Julian Oscillation (MJO; Madden and Julian, 1972), the global frictional torque and the global mountain torque were combined to construct four distinct phases of a global synoptic dynamic model (GSDM) of the atmosphere.

In this study, an objective definition of the GSDM is derived for monitoring and prediction applications. This will involve combining the MJO, as defined by Wheeler and Hendon (2004 hereafter WH), with the global wind oscillation (GWO) as defined by the global relative atmospheric angular momentum (AAM) and its time tendency. Although both "oscillations" produce signals in AAM, the MJO signal develops through tropical convective forcing and meridional wave energy dispersion while the GWO signal is dominated by mid-latitude mountain forcing and zonal wave energy dispersion. Additionally, the GWO life cycle includes phases that resemble the circumglobal teleconnection pattern studied by Branstator (2002).

A case study is used to introduce the GWO. The main purpose of the case study is to illustrate a subseasonal event with a large signal in the GWO phase space but a small and irregular one in the MJO's space. Observations of lead and lag suggest brief episodes of projection on the MJO may actually be forced by circulation anomaly fields linked to global mountain torques and zonal mean momentum transports.

In Section 3, we examine the relationship between the MJO and the GWO and contrast their spectra and cross-spectra. We show that the MJO is embedded within the GWO but that independent mid-latitude processes are important along with tropical convective forcing. In Section 4 the phase-space plots for both oscillations are introduced and a summary of the MJO and GWO features is presented. The phase plots are then used to study the period from April-May 2007. The results show tropical convective forcing, while important, had weak projection on the MJO while the global wind oscillation (GWO) projections were large and primarily forced by extreme mountain torque events. The case study relationship between the global indices and the zonal mean flow anomalies is also examined. Finally, a successful week 2 prediction of a western USA trough in late May 2007 is related to a particular portion of the GWO phase space, one where prediction models often struggle and have low predictability in the 1-3 week forecast range. Summary and conclusions are in Section 5.

2. Data sets and calculations

The NCEP/NCAR reanalysis-1 (Kalnay et al., 1996) is the primary dataset used in the study. The global integral of relative AAM (M_R) and its time tendency are computed as described by Weickmann and Sardeshmukh (1994) using daily averages of 4x daily data. It is defined as

$$M_R = \int_{-\pi/2}^{\pi/2} a\cos\varphi d\varphi \int_0^{2\pi} ad\lambda \int_0^{p_s} m_r dp / g \qquad (1)$$

where m_r = a u cos φ, a is the earth's radius, u is zonal velocity, φ is latitude, p_s is surface pressure and g is gravity. The global tendency (dM_R/dt) is estimated from the M_R time series using a 4th order finite difference scheme. The anomalies are computed relative to a 1968-96 climatology and are standardized using 5-day average data from 1968-2006. The standard deviations based on the entire record are shown in Table 1. Tests using the 365 day computed annual cycle of standard deviations versus one value for the entire year did not substantially change the results.

Since the M_R units are unfamiliar to some readers a conversion to zonal wind units is provided in Table 1, where the global mean (uniform) zonal wind corresponding to a global relative AAM value is given by

$$\bar{u} = M_R g / \pi^2 a^3 p_s \quad . \qquad (2)$$

An application example is the seasonal cycle where M_R is characterized by an annual mean of 1.4×10^{26} kgm^2s^{-1} and an average annual range from 1.4×10^{26} kgm^2s^{-1} to 1.7×10^{26} kgm^2s^{-1}. The equivalent values from (2) are 5.4, 4.6 and 6.5 ms^{-1}, respectively. (One could also define a global mean of u cos φ, which would imply a meridional profile of the zonal mean zonal wind.)

Table 1: Standard deviations for the global wind oscillation (GWO) In AAM units and equivalent global mean zonal wind units		
	GWO1 (M_R)	GWO2 (dM_R/dt)
Daily data	1.25×10^{25} kgm^2s^{-1} 0.5 ms^{-1}	1.84×10^{19} kgm^2s^{-2} 0.07 m s^{-1} day^{-1}
Pentad data	1.24×10^{25} kgm^2s^{-1} 0.5 ms^{-1}	1.38×10^{19} kgm^2s^{-2} 0.05 m s^{-1} day^{-1}

Table 1. See text and (2) for conversion between units. Pentad averaging does not remove much noise from the M_R time series but it does from dM_R/dt, decreasing its standard deviation by 25%. This is consistent with their e-folding times.

Similarly, for a latitude band one can define

$$[\{m_r\}]_\varphi = \int_\varphi^{\varphi+\Delta\varphi} a\cos\varphi\, d\varphi \int_0^{2\pi} a\, d\lambda \int_0^{p_s} m_r\, dp / g \qquad (3)$$

and relate the value to a zonal and vertical mean zonal wind

$$[\{u\}]_\varphi = [\{m_r\}]_\varphi\, g \Big/ 2\pi\cos^2\varphi\,\Delta\varphi\, a^3 p_s . \qquad (4)$$

Thus, an $[\{m_r\}]_\varphi$ anomaly of $1.0\text{x}10^{24}$ kg m^2 s^{-1} corresponds to a vertical and zonal mean zonal wind anomaly of 2.8 m/s at 30° and 8.4 m/s at 60°, where $\Delta\varphi$ is ~1.9° for a 192x94 Gaussian grid. For $[\{\partial m_r/\partial t\}]_\varphi$, an integrated anomaly of $1.0\text{x}10^{18}$ kg m^2 s^{-2} corresponds to a vertical and zonal mean zonal wind tendency of ~0.2 m s^{-1} day^{-1} at 30°.

Finally, the extreme GWO events during the case study had equivalent anomalies of +/- 1 ms^{-1} for the global mean zonal wind and +/- 5.6 ms^{-1} for $[\{u\}]_\varphi$ at 30°. For the tendency, equivalent anomalies are +/- 0.15 ms^{-1}day^{-1} for the global mean and +/- 0.8 ms^{-1}day^{-1} for $[\{\partial u/\partial t\}]_\varphi$. The mountain torque from individual mountain ranges like the Rockies, the Plateau of Tibet and the Andes can contribute > 50% of the tendency.

3. The Madden Julian Oscillation versus the Global Wind Oscillation: cross-spectral and spectral analysis

WH defined an empirical measure of the MJO from the first two EOFs of a multivariate field consisting of a 15N-15S average of the 200 mb zonal wind, the 850 mb zonal wind and OLR. They refer to the two EOF time series as RMM1 and RMM2. Using an analogous approach, the GWO is defined by two dynamically related quantities: M_R and

dM_R/dt, which will be referred to as GWO1 and GWO2 respectively. Figure 1 shows sample 120-day time series for the MJO and the GWO during Jan-Apr 2006. Multiple time scales are readily apparent even in this short record. The GWO has 10, 30 and 60 day trough to trough or peak to peak variations while the MJO's are more like 20, 30 and 40-50 days.

Not surprisingly the MJO and GWO indices are correlated. The MJO induces torques both within and outside tropics as it moves eastward with the remote component linked to meridional Rossby wave dispersion. Similarly the GWO can excite tropical convection anomalies through the large-scale tropical wind and sea level pressure anomalies that accompany the friction torque or the dispersion of extratropical Rossby wave energy into the tropics that accompany the mountain torque. The relation between the two is summarized in Table 2 where cross-spectral results for 20-120 day and 30-80 day 1/frequency bands are shown. The latter and 30-60 day bands have been used to define the MJO. All indices have only the mean and mean seasonal cycle removed, thus the RMMs are not exactly as defined by WH.

Table 2. Cross spectrum analysis between the MJO and GWO
Entries: coherence-squared (correlation), phase in radians

Frequency band	20-120 day periods		30-80 day periods	
"Oscillations"	RMM1 (0.58)	RMM2 (0.65)	RMM1 (0.45)	RMM2 (0.50)
GWO2 (0.4, 0.25)	0.2 (.45), 0.2	0.27 (.52), -1.3	0.25 (.50), 0.3	0.34 (.58), -1.3
GWO1 (0.28, 0.22)	0.21 (.46), 1.9	0.33 (.57), 0.2	0.26 (.51), 1.8	**0.38 (.62), 0.3**

Table 2. Cross-spectral analysis is shown between the MJO and the GWO for two frequency bands using daily, standardized anomalies. Record length is the 9862 days from 1979-2005. The largest [coherence-squared (correlation), phase] values are shown in bold where GWO1 (M_R) is correlated with RMM2 in the 30-80 day band. The numbers following the index identification are the fractional variance contained in the frequency bands (e.g., (0.58) means 20-120 day band contains 58% of the variance). For the GWO in column 1, the numbers in parentheses refer to the variance fraction for 20-120 day and 30-80 day bands, respectively.

In general there is little difference in the results between the two bands. The strongest relationship is between GWO1 and RMM2 with a nearly in-phase, maximum correlation of 0.62 at 30-80 days (bold in Table 2). The result generally confirms Madden's (1987) observation of the relationship between M_R and the MJO'S tropical convection but it is also influenced by the 200 zonal wind component of RMM2, not only the convective component. In any case, the result will be used in the next section to justify a GWO phase space where M_R is plotted along the y-axis (with RMM2) and dM_R/dt is plotted along the x-axis (with RMM1). The latter relationship is also relatively large for both bands (Table 2) and consistent with the fact that RMM1 and RMM2 are in-quadrature.

Fig. 2 shows frequency spectra of the two components of the MJO and GWO. The comparison of the observed spectra to the red noise background emphasizes the primary difference between the two phenomena. The MJO is an oscillation with a peak in both RMM spectra at around 45 days. The GWO on the other hand shows two red noise processes; one with fast (2 days) and the other with slow (14 days) e-folding times that effectively bracket the MJO's 30-80 day variance band giving considerable overlap in their spectral signature.

There is some structure in the GWO spectra worth commenting on. GWO1 has a nearly significant peak at ~52 days tilted toward 30-60 days and this likely reflects MJO forcing. The "peak", however, is clearly on top of a red noise background with a 14 day decay time scale, a separate phenomenon from the MJO. The GWO2 (dM_R/dt) spectrum forms a plateau of variance from 5-40 days with a hint of separate maxima from 5-15 days and 25-40 days. These are significant at the 95% level, at least with respect to the chosen red noise backgrounds, which are determined from the decay time scales of the M_R and dM_R/dt time series. The 5-15 day band reflects the global mountain torque produced by synoptic wavetrains moving over the mountains (Iskenderian and Salstein, 1998, W03). Such events induce small but discernible responses in global AAM as can be seen in Fig. 1a. The 25-40 day band is also dominated by the mountain torque (WRP), which has 2-3

times the variance of the frictional torque in this frequency range. This band is the primary driver for both MJO and non-MJO portion of the GWO.

While a portion of the GWO variance is related to the MJO, there are many subseasonal events where the mountain torque is much larger than the frictional torque. WRP discussed the global and zonal aspects of global mountain torque events while W03 illustrated the horizontal patterns that accompany them. The similar frequencies involved with the MJO and this mountain-frictional torque adjustment process suggest the possibility of mutual excitation and interaction.

4. Phase Space Plots

The phase space plots introduced by WH are an efficient and objective way to monitor the MJO. They are being applied widely for diagnostic research and by operational centers to monitor their model's prediction of the MJO (http://www.cdc.noaa.gov/MJO/Forecasts). In this section, we introduce a similar phase plot for the GWO and then summarize some key results from composites computed from the MJO and GWO indices.

To start, the WH phase plot for the MJO is reproduced in Fig. 3 showing phases 1-8 defined as eight 45° segments in the 360° phase space. The text boxes inside the circle of arrows highlight important events when compositing on the RMMs including the location of tropical convection and changes in the large scale circulation. Outside the circle of arrows, the components of the GWO are shown when compositing on the RMMs. The orbits rotate counter-clockwise (CCW) during an eastward-propagating MJO but can rotate clockwise for a variety of reasons including tropical waves (Roundy et al., 2008) and SST anomalies. Fig. 3 depicts a familiar time-sequence of active tropical convective regions and large scale circulation changes during a MJO orbit.

Figure 4 illustrates the phase space plotting format for the GWO. The phases match those already defined by WH for the MJO. This will simplify real time monitoring and

comparing composites in the companion paper. AS mentioned previously, the relatively large coherence-squared between GWO1 and RMM2 is used to define the relationship between the two phase spaces. The dashed arrows show a schematic orbit in the GWO phase space, which can only rotate CCW and need not be oscillatory. Westerly and easterly flows are exchanged with the solid earth during an orbit.

Inside the arrows, important events in the circulation and related surface torques are again shown while outside the arrows composites for tropical convection are shown. Along the GWO phase space trajectory from 8 to 1, a negative global frictional torque is followed by negative global mountain torque and together these processes give a strong negative AAM tendency that means westerly momentum is being removed from the atmosphere. A regional-scale response is for the extended North Pacific Ocean jet to collapse, often leading to a trough in the western USA (see the case study discussed in Section 5). Monitoring experience suggests that the global numerical models perform poorly in these situations.

During GWO phases 8 to 1 the tropical forcing is propagating eastward from the region of South America to over the Indian Ocean. As convection continues to shift into the Indian Ocean, poleward AAM transports develop in the zonal mean at around 35°N (and 35°S). This favors a northward shifted storm track and a circumglobal teleconnection (Branstator 2002) pattern of anomalous mid-latitude ridges with inter-hemispheric symmetry by phase 3. The latter base state is also typical of La-Nina. The ability to anticipate certain phenomena or processes provides an added dimension to a real time monitoring activity devoted to extended range weather and climate forecasts.

5. Case Study: April-May 2007

a. Phase space plots

Fig. 5 is the MJO phase plot for the 59 days from 28 March to 25 May 2007 with a 5-day running mean applied. In contrast to the standard plot (e.g., WH), interannual variations

are retained. This causes the center of the orbits to shift slightly (~0.5 sigma) toward the "La Nina" phases 3-4. The MJO activity shows three coherent episodes where projections of > one sigma or systematic eastward propagation occurred. These were interrupted by two periods with nearly zero signals, 10-22 April and 8-15 May. The plot starts with a MJO that developed over the Indian Ocean in mid-March 2007 and has now moved past the maritime continent around phase 5. From there, the MJO moves toward phase 1 before weakening around 10 April. The standard MJO phase plot (not shown) has > 1 sigma projections during this time. Another weak event develops at the end of April 2007 at phase 2-3, moves east briefly to phase 4-5, weakens further ~6 May, but then re-intensifies to > 1 sigma at phase 7 as it moves east through the "West. Hem. and Africa".

The annotations on Fig. 5 depict four periods with extreme dM_R/dt anomalies. Together they produce two ~30 day GWO oscillations whose orbits in phase space will be discussed shortly. The mountain torque contributes substantially to the extreme tendencies. In Fig. 5, the two periods (10-22 April and 8-15 May) with near zero MJO but extreme GWO2 projection are highlighted using thickened line segments. The thickened segments occur just before MJO convection re-intensifies over the Indian Ocean in late April and over the western Pacific in mid-May 2007. The connection is highlighted using heavy black arrows. The composites to be presented in the companion paper confirm these relationships between the GWO tendency and the subsequent tropical convection anomalies.

Turning to the GWO, Fig. 6 shows its phase plot for the same period as the MJO in Fig. 5. The same dates have thickened line segments applied. Two prominent orbits are seen during the 59-day period; one from 28 March to 25 April (29 days) and the other from 26 April to 26 May (31 days). The first is a single orbit while the second combines a fast and slow orbit. On average the orbits are centered slightly away from zero toward phase 3-4 signifying a persistent negative global AAM anomaly, characteristic of a La Nina circulation state.

The regularity of the GWO orbits contrasts with the more variable MJO projection seen in Fig. 5. The relationship between the GWO and MJO projections discussed in Fig. 5 is also evident in Fig. 6. Indian Ocean convection (IO) follows the extreme negative tendency in mid-April and west Pacific Ocean (wPO) follows the extreme positive tendency in early May. On the other hand, the other two extreme tendencies in late May and early April are more integrated with the MJO convection anomalies so that forcing and response relative to mid-latitude or tropical forcing is less clear-cut.

For example, early in the first orbit, both the eddies that responded to west Pacific tropical forcing and to a positive mountain torque from the Plateau of Tibet were easy to follow in a sequence of daily weather maps. Atmospheric Rossby wave dispersion, linked to both forcing mechanisms in a rapid sequence, contributed to a zonal mean southward momentum flux across 40N. This is consistent with the GWO feature seen at phase 6 on Fig. 4 and will also be evident in the evolution of zonal AAM described in the next section. It is just one example of a process that can be anticipated when the signals in the GWO or the MJO are large and appear to be making a circuit or orbit.

Realistic subseasonal signals are clearly complex and it is not easy to disentangle forcing-response-feedback. The main point is that subseasonal events evolve through the mutual interaction between tropical convection and mid-latitude mountain-torque dominated processes. For the zonal mean, the tropics and major mountainous regions are linked via meridional momentum transports across 35N (35S). In the next section the variations of the zonal mean circulation are related to M_R, while dM_R/dt is shown to be dominated by mountain torques from three primary regions: the Plateau of Tibet, the Rockies of North America and the Andes of South America.

b. Zonal-vertical integrals

Figure 7 presents the M_R time series and the $[\{m_r\}]_\varphi$ anomalies for the same time period as Fig. 6. The bottom panel shows the two orbits in time series form while the top panel

shows the related zonal anomalies. The GWO phases and the location of positive tropical convection anomalies have been marked on the bottom time series. Comparing the top and bottom panels shows the orbits are produced by variations in the zonal mean zonal flow, roughly in the region between 30N-30S. The long-term mean anomalies (>60 days) are negative in this region so Fig. 7a shows a pattern of easterly flow anomalies interspersed with near zero anomalies; i.e., not westerly ones. The anomalies are shifting poleward, a feature emphasized by highlighting the axis of positive AAM tendency in Fig. 7a. The first orbit in early April has a fast, discontinuous northward shift in the positive tendency while the second in early May is slow and more coherent. These shifts occur as AAM temporarily recovers from the low values seen in late March and late April 2007.

Meridional momentum transports are the primary forcing for the poleward shifts and while advection by tropical mass circulations may initiate the events, they are extended poleward and in time by the mountain torque and favorable mid-latitude eddy structures. Within the general Fig. 7a pattern of negative zonal mean zonal flows, there are time periods and latitudes where westerly wind anomalies develop and persist. In the first orbit this occurs near 35N while in the second it occurs more weakly near 20N and 15S. These are related to a combination of the strong meridional momentum fluxes and large positive mountain torques. The weak but positive global anomalies seen in Fig. 7b develop because of these zonal mean westerly wind anomalies. As shown below, the zonal anomalies develop in latitude bands that contain the Asian, North American and South American mountains. Although they are embedded in strong meridional fluxes of zonal momentum, the mountains act as additional momentum sources that have regional impacts downstream and can even change the zonal mean or global zonal flow.

Figure 8 shows the zonal-vertical and global integral of the relative AAM tendency corresponding to Fig. 7. The anomaly budget is dominated by the flux convergence of AAM followed by the mountain torque, the frictional torque and the coriolis torque in order of importance (WKS, W03). The purpose here is not to analyze the complete budget but rather illustrate the timing of important physical processes during the two

GWO orbits. Recall that the orbits start after maximum easterly flow anomalies have been established around 20N and 20S. The Fig. 8 top panel shows the negative tendencies that create these anomalies and the positive tendencies that follow and weaken them after the start of the orbits.

Despite the complicated structure of the tendency field, a careful comparison with Fig. 7 confirms a poleward movement of discrete negative and positive tendency events, and these have been highlighted on the figure. They appear to emanate from north of the equator in the Northern Hemisphere. The progression of negative and then positive events is especially well defined during the second orbit. The flux convergence of AAM is the primary driver for this behavior (WKS). Anomalous meridional mass circulations forced by either tropical convection or eddy momentum fluxes likely drive the tropical-subtropical tendencies while eddy momentum fluxes become the dominant driver at high latitudes. The suggestive temporal connection in zonal mean flow anomalies for periods of 1-3 months between the tropics and polar latitudes is not well understood dynamically (Chang, 1998; Feldstein, 1998; Lorenz and Hartmann, 2001; Lee et al., 2007) but often observed. On average, the MJO composite based on the RMMs (not shown) only gives propagation of zonal mean zonal wind anomalies to 20N (20S) so it provides no full explanation. Possibly a combination of the GWO and MJO are important, and this will be examined in a follow-up paper on zonal and regional composites. In general the interplay between the momentum transports, the mountain torque and tropical convective forcing is still poorly understood.

The flux convergence of AAM cannot produce a global AAM tendency but it can lead to zonal wind anomalies that then produce zonal and global mountain torques. The two large momentum transport events referred to previously are marked on Fig. 8 and coincide with the two large global tendencies seen in the bottom panel. The meridional transports are directed southward in early April and early-mid May. The colored curves in the bottom panel confirm that mountain torques due to North American and Asian topography make an important contribution to the first tendency and that South American

and Asian topography contribute to both the smaller tendency at the start of the second orbit and the much larger tendency 10 days later.

Quantitative data analysis and diagnostic modeling is required to understand the complete progression of the AAM tendency curve seen in Fig. 8. But for forecasting purposes, Fig. 3 and 4 supply an expected sequence of events that can be monitored and anticipated, thereby helping to evaluate model predictions and a probable future atmospheric state. In this case study, the events that typically accompany phases 8-1 were used to forecast a western USA trough that developed ~20-23 May leading to severe local storms on the Great Plains and significant temperature and precipitation anomalies across the country. The initial forecast was based on the size of the positive tendency during ~10 May while in phase 4-5 and the fact that one orbit had already occurred. A well known synoptic sequence accompanies phases 8-1: the Pacific jet stream strengthens, extends east and then breaks down leaving a trough over the southwestern USA. The acceleration of the zonal mean jet during the two orbits is seen by the large positive zonal AAM tendencies around 30N in Fig. 8a. Of course the forecast challenge is to determine when or if the jet will break down, and this involves impacts from the synoptic as well as the interannual time scales.

6. Summary and Conclusions

The global wind oscillation (GWO) has been introduced as an additional aid to monitor and help understand subseasonal variations of the global atmospheric circulation. It is defined using global relative AAM and its tendency and when plotted in a phase space diagram eight phases are defined. Frequency spectra were used to contrast the ~45 day oscillations of the MJO with the multiple time scale, red noise behavior of the GWO.

A case study from April-May 2007 compares the time evolution of the GWO and the MJO. The GWO was strong and coherent throughout the case compared to a transient and weak projection for the MJO. The GWO variations were linked to zonal mean flow anomalies in tropical regions between 30N-30S. During two well-defined GWO orbits,

anomalies of one sign in this latitude band are replaced with anomalies of opposite sign while the original anomalies shift poleward. Mountain torques embedded within strong meridional momentum fluxes contributed additional momentum sources and sinks in specific latitude bands and also had a major contribution to the global relative AAM tendency. In time-latitude plots, zonal mean westerly wind anomalies were observed to emanate from the latitude bands that contain major mountain ranges, especially Asia and South America.

The MJO can produce a signal in the GWO as shown by the moderate correlation between them. However, it was argued that a separate mode of variation dominates the GWO tied to the atmospheric circulation adjusting to large or clustered mountain torque events. Both the MJO and the GWO produce zonal wind anomalies in the tropical band and thus it is reasonable to suppose the oscillations can interact and excite one another. These "oscillations" are being monitored in real time as the primary components of the global synoptic dynamic model introduced by Weickmann and Berry (2007). Understanding the dynamical processes explained by the GWO allows for a more sophisticated evaluation of the numerical models as part of a complete forecast process.

A companion study uses the GWO to construct eight phase composites of zonal mean and global teleconnection patterns. These are contrasted with the MJO's composite patterns. Fig. 9 shows an example of a partial sequence from both the GWO and MJO life cycles during December-January-February. The sequence focuses on the breakdown of a strong jet stream anomaly that develops over the North Pacific Ocean in both cases. There is about 4-8 days between the phases. The composite differences confirm the GWO is dominated by zonal Rossby wave dispersion while the MJO has prominent meridional dispersion of Rossby waves. For the MJO (Fig. 9a), the jet anomalies are part of a meridional Rossby wavetrain, established over 1-3 weeks as convection anomalies move into the western and central tropical Pacific. The pattern breaks down when convection anomalies propagate into the western hemisphere. For the GWO (Fig. 9b), the jet anomalies extend farther eastward in response to the Asian mountain torque and weaken in response to anticyclonic or cyclonic wave breaking events over the mid-

latitude east Pacific (not shown). This is followed by the slow dispersion of Rossby wave energy into the tropical western hemisphere.

A comprehensive analysis of both the MJO and GWO life cycles, including their sensitivity to the seasonal cycle and ENSO is planned in future work. The phase spaces and accompanying composites are available on the web to help monitor and evaluate the global weather-climate situation (http://www.cdc.noaa.gov/map/clim/gsdm.composites.shtml).

Acknowledgements.

EKB expresses appreciation to Larry J. Ruthi, MIC, NOAA/NWS/WFO Dodge City, Kansas, for his support of the project. Encouragement and support from Robin Webb and Randy Dole are also appreciated.

References

Anderson, J., and R. Rosen, 1983: The latitude-height structure of 40–50 day variations in atmospheric angular momentum, *J. Atmos. Sci.*, *40*, 1584–1591.

Branstator, G. W., 2002: Circumglobal teleconnections, the jet stream waveguide, and the North Atlantic Oscillation. *J. Climate.,* **15,** 1893-1910.

Chang, E. K. M., 1998: Poleward-propagating angular momentum perturbations induced by zonally symmetric heat sources in the tropics. J. Atmos. Sci., 55, 2229-2248.

Dickey, J., M. Ghil, and S. Marcus, 1991: Extratropical aspects of the 40–50 day oscillation in length-of-day and atmospheric angular momentum, *J. Geophys. Res.*, *96*, 22,643–22,658.

Feldstein, S., 1998: An observational study of the intraseasonal poleward propagation of zonal mean flow anomalies. *J. Atmos. Sci.*, **55**, 2516-2529.

Ghil, M., and S. Childress, 1987: *Topics in Geophysical Fluid Dynamics: Atmospheric Dynamics, Dynamic Theory and Climate Dynamics*, 485 pp., Springer, New York.

Ghil, M., and A.W. Robertson, 2002: "waves" vs. "particles" in the atmosphere's phase space: A pathway to long-range forecasting? The Arthur M. Sackler Colloquium "Self-organized complexity in the physical, biological, and social sciences" March 23-24, 2001 at Arnold and Mabel Beckman Center, Irvine, CA. Reprint: Institute of Geophysics and Planetary Physics, 3839 Slichter Hall, Iniversity of California, 405 Hilgard Ave, Las Angeles, CA 90095-1567

Iskenderian, H. and D.A. Salstein, 1998: Regional sources of mountain torque variability and high-frequency fluctuations in atmospheric angular momentum. *Mon. Wea. Rev.*, **126**, 1681-1694.

Jin, F.-F., and M. Ghil, 1990: Intraseasonal oscillations in the extratropics: Hopf bifurcation and topographic instabilities. *J. Atmos. Sci.*, **47**, 3007-3022.

Kalnay, E., and co-authors, 1996: The NCEP/NCAR 40-year reanalysis project: *Bull. Amer. Meteor. Soc.*, 77, 437-471.

Hendon, H. H., 1995, Length of day changes associated with the Madden-Julian Oscillation. *J. Atmos., Sci.*, **52**, 2373-2383.

Langley, R. B., R. W. King, I. Shapiro, R. Rosen and D. Salstein, 1981: Atmospheric angular momentum and the length of day: a common fluctuation with a period near 50 days. *Nature*, **294,** 730-732.

Lee, S., S.-W. Son and K. Grise, 2007: A mechanism for the poleward propagation of zonal mean flow anomalies. *J. Atmos. Sci.*, **64**, 849-868.

Lorenz, D. J. and D. L. Hartmann, 2001: Eddy-zonal flow feedback in the southern hemisphere. *J. Atmos. Sci.*, **58**, 3312-3327.

Lott, F., A.W. Robertson and M. Ghil, 2004: Mountain torques and Northern-Hemisphere low-frequency variability. Part I: Hemispheric aspects. *J. Atmos. Sci.*, **61**, 1259-1271.

Lott, F. and F. D'Andrea, 2005: Mass and wind axial angular-momentum responses to mountain torques in the 1-25 day band: Links with the Arctic oscillation. *Q, J. R. Meteorol. Soc.*, **131**, 1483-1500.

Madden, R. A., and P. R. Julian, 1972: Description of global-scale circulation cells in the tropics with a 40–50 day period. *J. Atmos. Sci.*, **29**, 1109–1123.

Madden, R.A., 1987: Relationships between changes in the length of day and the 40- to 50- day oscillation in the tropics. *J. Geophys. Res.*,**92**, 8391-8399.

Madden, R.A., 1988: Large intraseasonal variations in wind stress over the tropical Pacific. *J. Geophys. Res.*, **93**, D5, 5333-5340.

Madden, R.A. and P. Speth, 1995: Estimates of atmospheric angular momentum, friction, and mountain torques during 1987-88. *J. Atmos. Sci.*, 52, 3681-3694.

Marcus, S.L., M. Ghil and J.O. Dickey, 1994: The extratropical 40-day oscillation in the UCLA general circulation model. Part 1: Atmospheric angular momentum. *J. Atmos. Sci.*, **51**, 1431-1446.

Marcus, S.L., M. Ghil and J.O. Dickey, 1996: The extratropical 40-day oscillation in the UCLA general circulation model. Part 1I: Spatial Structure. *J. Atmos. Sci.*, **53**, 1993-2014.

Peixoto, J. P. and A. H. Oort, 1992: *Physics of Climate* (Chapter 11), Springer-Verlag New York, Inc., 520 pp.

Roundy, P., C. Schreck and M. Janiga, 2008: Contributions of convectively coupled equatorial Rossby waves and Kelvin Waves to the real-time multivariate MJO indices. *Mon. Wea. Rev.*, submitted.

Sardeshmukh, P.D. and P. Sura, 2008: Reconciling non-Gaussian climate statistics with linear dynamics. *J. Climate*, in press.

Wallace, J.M. and D.S. Gutzler, 1981: Teleconnections in the geopotential height field during Northern Hemisphere winter. *Mon. Wea. Rev.*, **109**, 784-812.

Weickmann, K. M., S.J.S. Khalsa and J. Eischeid, 1992: The atmospheric angular momentum cycle during the tropical Madden-Julian Oscillation. *Mon. Wea. Rev.*, **120**, 2252-2263.

Weickmann, K.M., 2003: Mountains, the global frictional torque, and the circulation over the Pacific-North American Region. *Mon. Wea. Rev.,* **131**, 2608-2622.

Weickmann, K.M., W.A. Robinson, and C. Penland, 2000: Stochastic and oscillatory forcing of global atmospheric angular momentum. *J. Geophys. Res.*, **105**, D12, 15543-15557.

Weickmann, K.M. and P.D. Sardeshmukh, 1994: The atmospheric angular momentum cycle associated with a Madden-Julian oscillation. *J. Atmos. Sci.*, **51**, 3194-3208.

Weickmann, K.M., G.N. Kiladis and P.D. Sardeshmukh, 1997: The dynamics of intraseasonal atmospheric angular momentum oscillations. *J. Atmos. Sci.*, **54**, 1445-1461.

Weickmann, K.M., and E. Berry, 2007: A synoptic-dynamic model of subseasonal atmospheric variability. *Mon. Wea. Rev.,* **135,** 449-474.

Wilks, D. S., 1995: Statistical methods in the atmospheric sciences. Volume 59, International Geophysics Series, Academic Press, 467pp.

Wheeler, M. C., and H. H. Hendon, 2004: An all-season multivariate MJO index: Development of an index for monitoring and prediction. *Mon. Wea. Rev.*, **132**, 1917-1932.

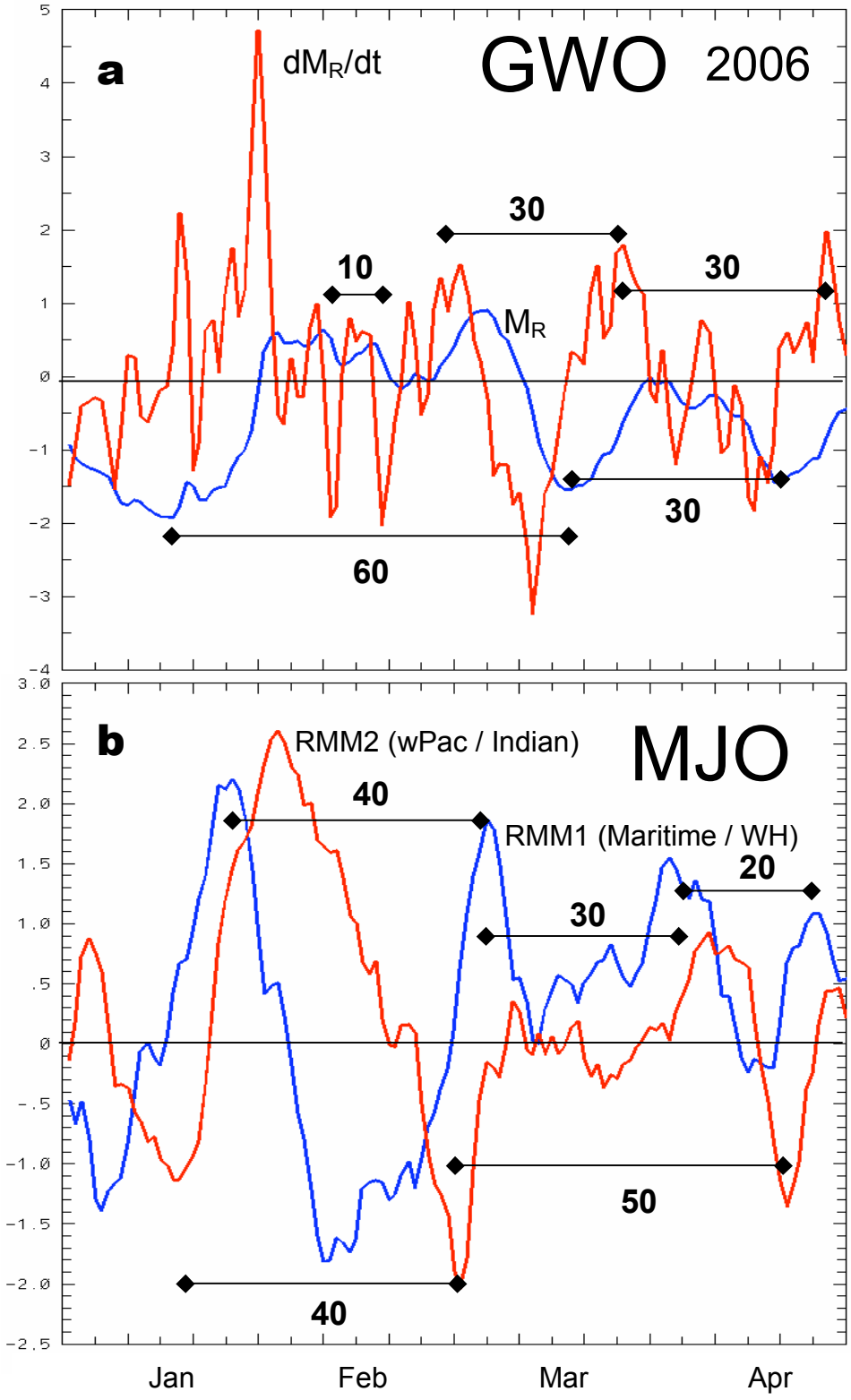

Fig. 1 The daily anomaly time series of: a. GWO1 (global relative AAM, blue line) and GWO2 (global relative AAM tendency, red line) for Jan-April 2006, b. RMM1 (blue) and RMM2 (red) for the same time period. The panels are annotated with the duration of some selected "oscillations".

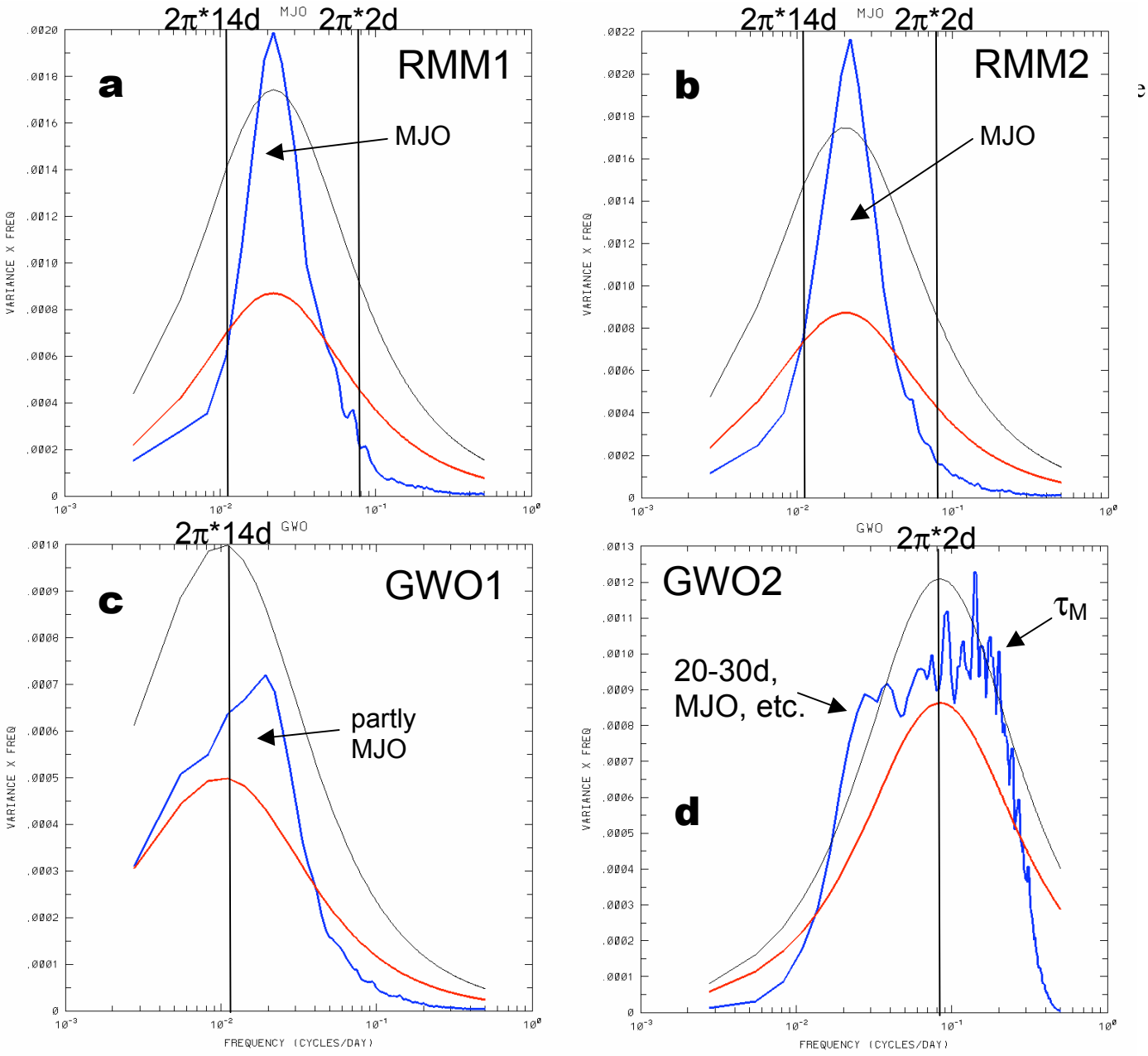

Fig. 2 The frequency spectra for the components of the MJO (a, b) and the GWO (c, d). The blue line is the observed spectrum, the red line is a red noise background (obtained from the e-folding time of the time series, see text) and the black line is the 95% level of the red noise spectrum. The spectra are plotted with log frequency as the abscissa and with frequency multiplied by variance as the ordinate. In this type of presentation there is a "peak" in a red noise spectrum whose location is proportional to the decay or e-folding time of the time series, with 50% of the variance contained on either side of this "peak". The degrees of freedom (dof) for the 95% levels were estimated from the number of data points divided by the e-folding time of the time series. This gives: a) 7.2 dof/bin, b) 7.2, c) 5.4 and d) 38 dof/bin.

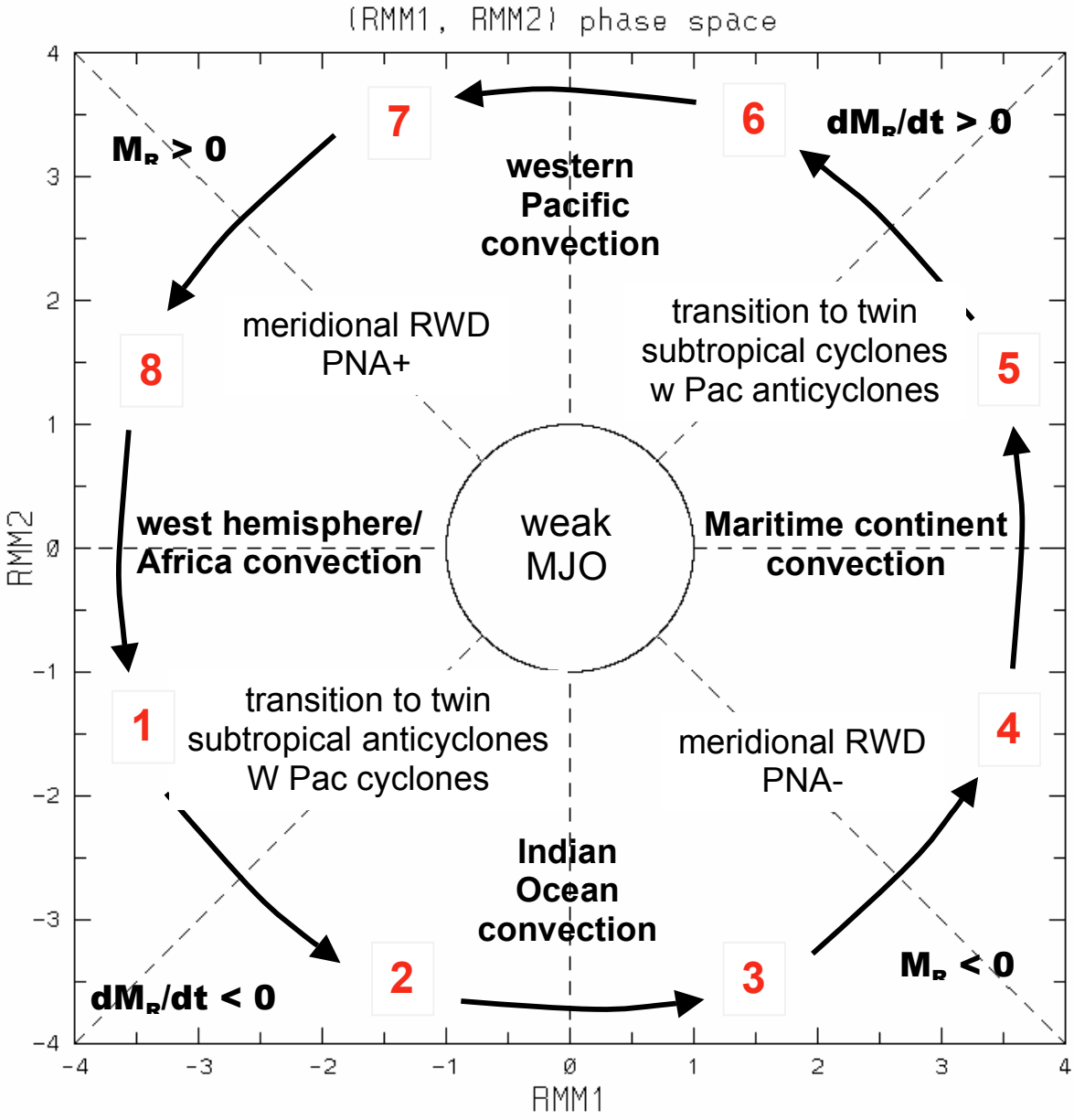

Fig. 3 The MJO phase plot as proposed by Wheeler and Hendon (2004). Two multivariate EOFs are used to define a 2-D phase space that is divided into 8 octants or segments, each covering 45°. The sequence of arrows depicts the rotation of the phase vector when an MJO is active and propagating eastward. For example, phase 2-8 would describe the development of convection over the Indian Ocean and its later demise over the western hemisphere. The text within and outside the sequence of arrows is based on DJF composites using the eight phases. The labels on the axes are standardized anomalies so the orbit shown by the sequence of arrows has an amplitude of 3.5 sigma.

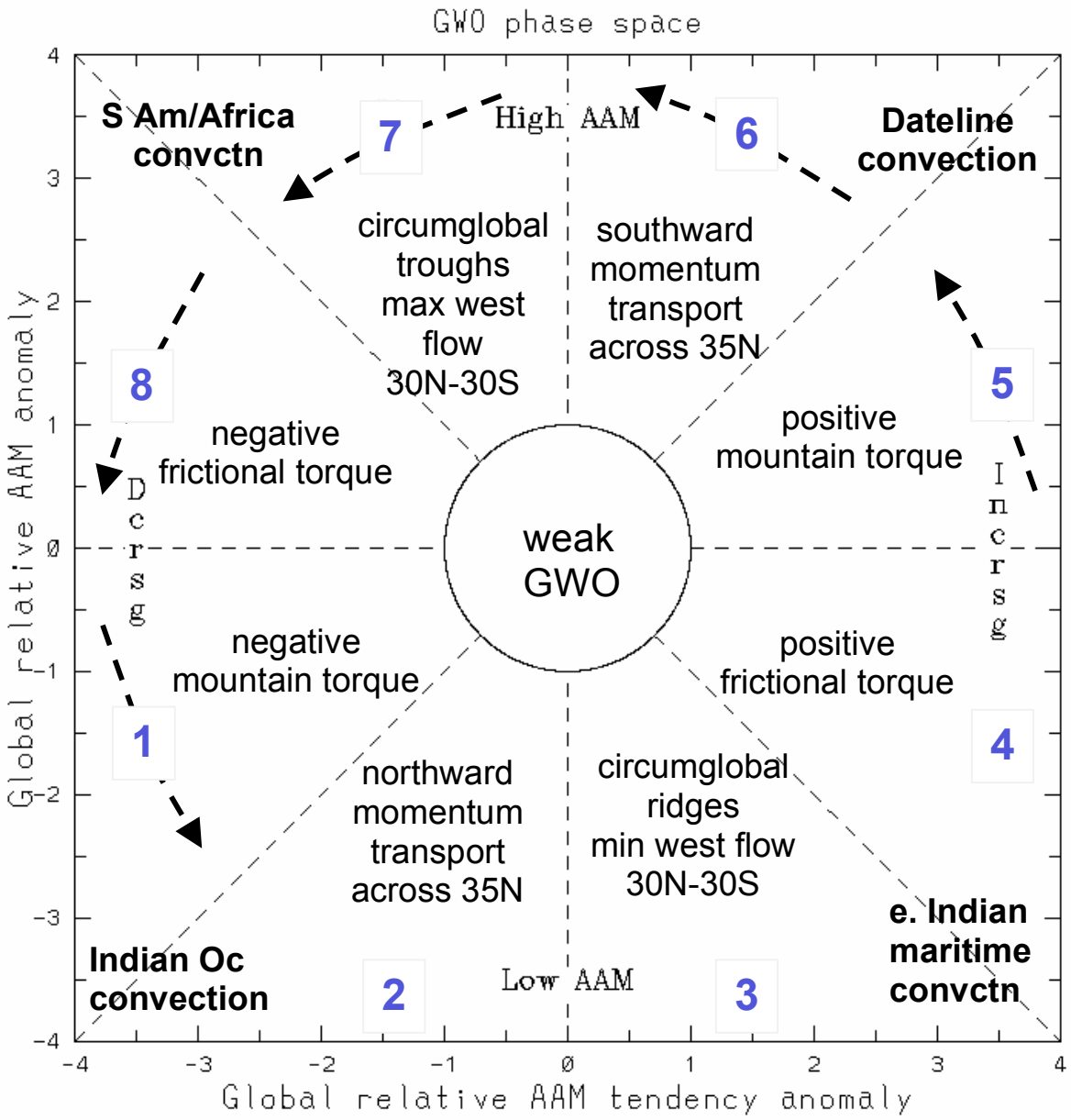

Fig. 4 The GWO phase plot as proposed in this paper. The MJO is embedded in the GWO but in addition the GWO is sensitive to mid-latitude processes like mountains and meridional momentum transports. The relation between the phase spaces was determined via cross-spectral analysis between the MJO and the GWO (see Table 2). The eight phases were defined to be the same between the two phase spaces. However, the GWO and MJO are not exactly "in-phase/quadrature" as is implied by the figure. Fast and slow time scales tend to be clustered in certain phases during the GWO thus phase moves faster or slower depending on its location in phase space. The dashed and truncated sequence of arrows emphasizes that the GWO is not oscillatory but on average gets excited and then decays. The text within the sequence of arrows is based on DJF composites for the eight phases. The text outside the sequence is also from composites but additionally shows the link of the GWO to tropical convection anomalies. Note the rapid movement of convection across Indonesia and the west Pacific during phase 3-6 compared with the MJO (Fig. 3).

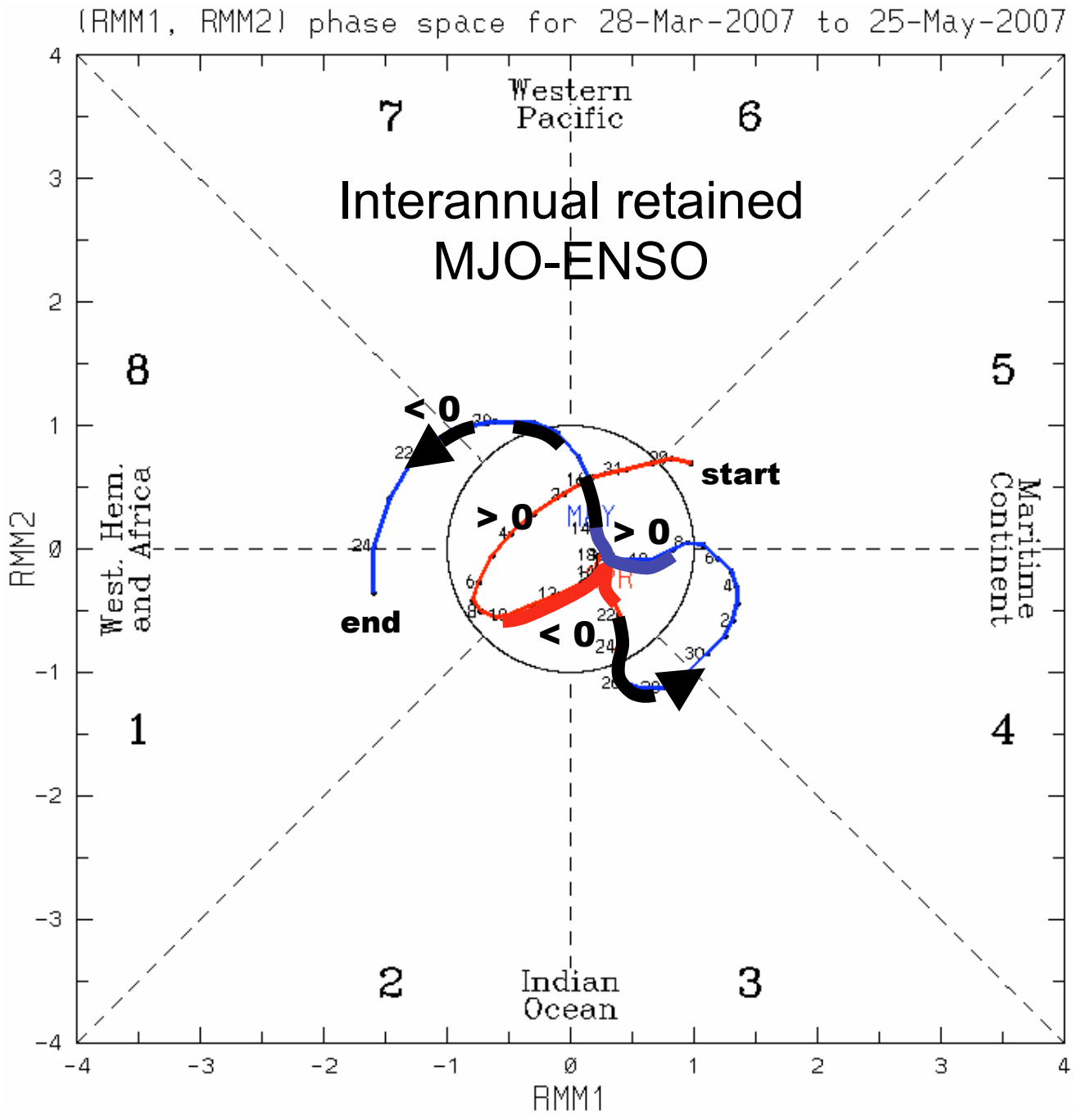

Fig. 5 The MJO phase plot for the 59-day period from 28 March to 25 May 2007. The red line with the dates track the first orbit of the GWO and the blue line the second. The interannual variations have been retained in this figure, so total anomalies have been projected onto RMM1 and RMM2. Since the climate was in a strengthening La Nina at this time the orbits are shifted slightly (~0.5 sigma) toward phases 3-4, which represent La Nina phases. Four cases of extreme global relative AAM tendency are marked on the figure alongside the time period when they occurred. See Fig. 6 for more details. Additionally the thickened red and blue lines denote two of these large tendency periods, which are seen to precede growth of the MJO projections during late April and late May.

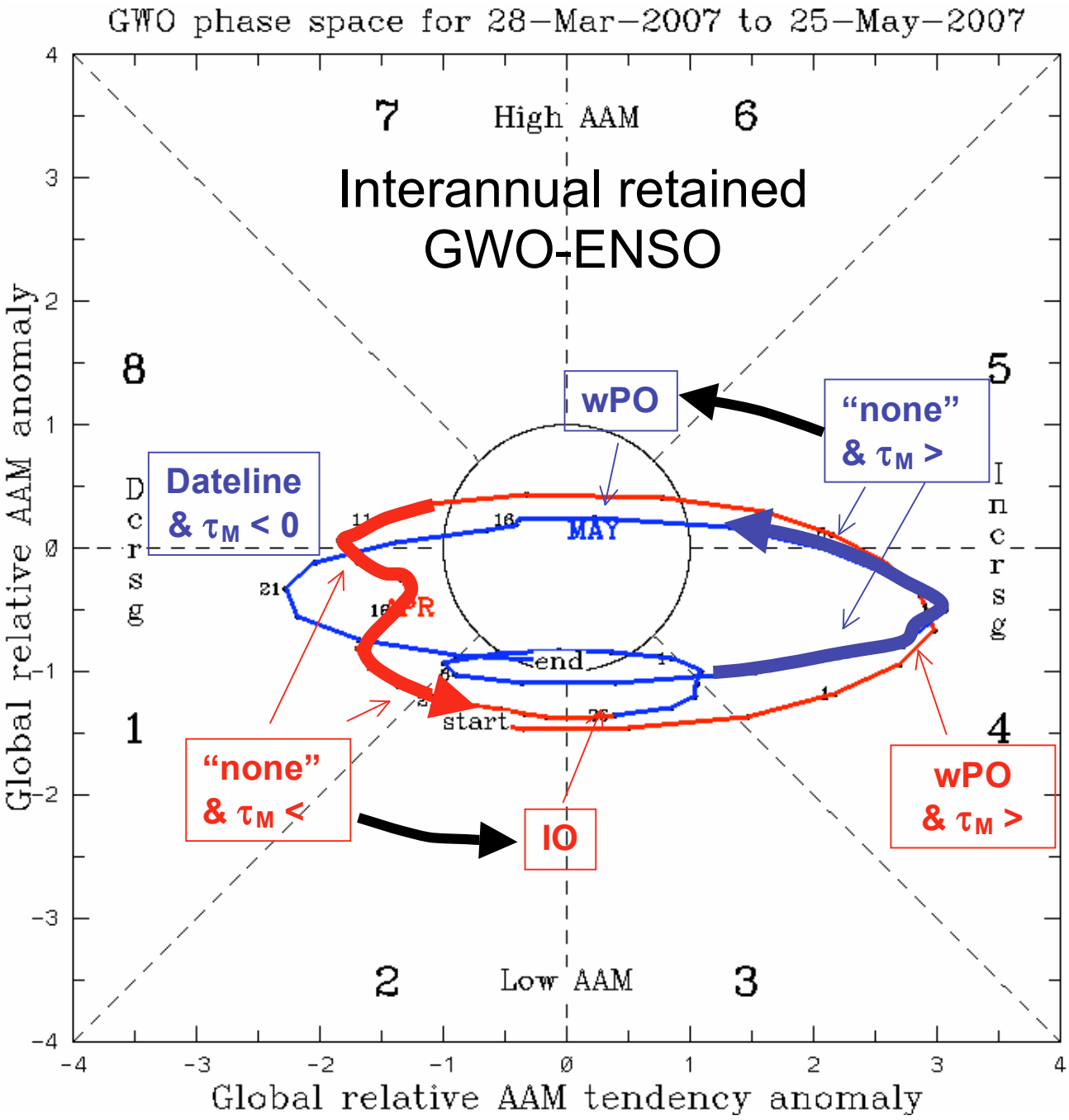

Fig. 6 The GWO phase plot for the 59-day period from 28 March – 25 May 2007. The red line with the dates track the first orbit of the GWO and the blue line the second. There are two ~30 day oscillations. The same time periods as Fig. 5 have thickened red and blue lines and show a ~3 sigma maximum for the blue positive tendency and a roughly -2 sigma minimum for the red negative tendency. The other two tendencies are also extreme. The location of the dominant tropical convection anomaly is labeled surrounding the orbits with the colors corresponding to the orbit colors. "None" means there were no well-defined large scale negative OLR anomalies present within the tropics. A link has been proposed between the two thickened tendency anomalies, which come primarily from the mountain torque, and the subsequent location of tropical convection (link denoted with heavy black arrows).

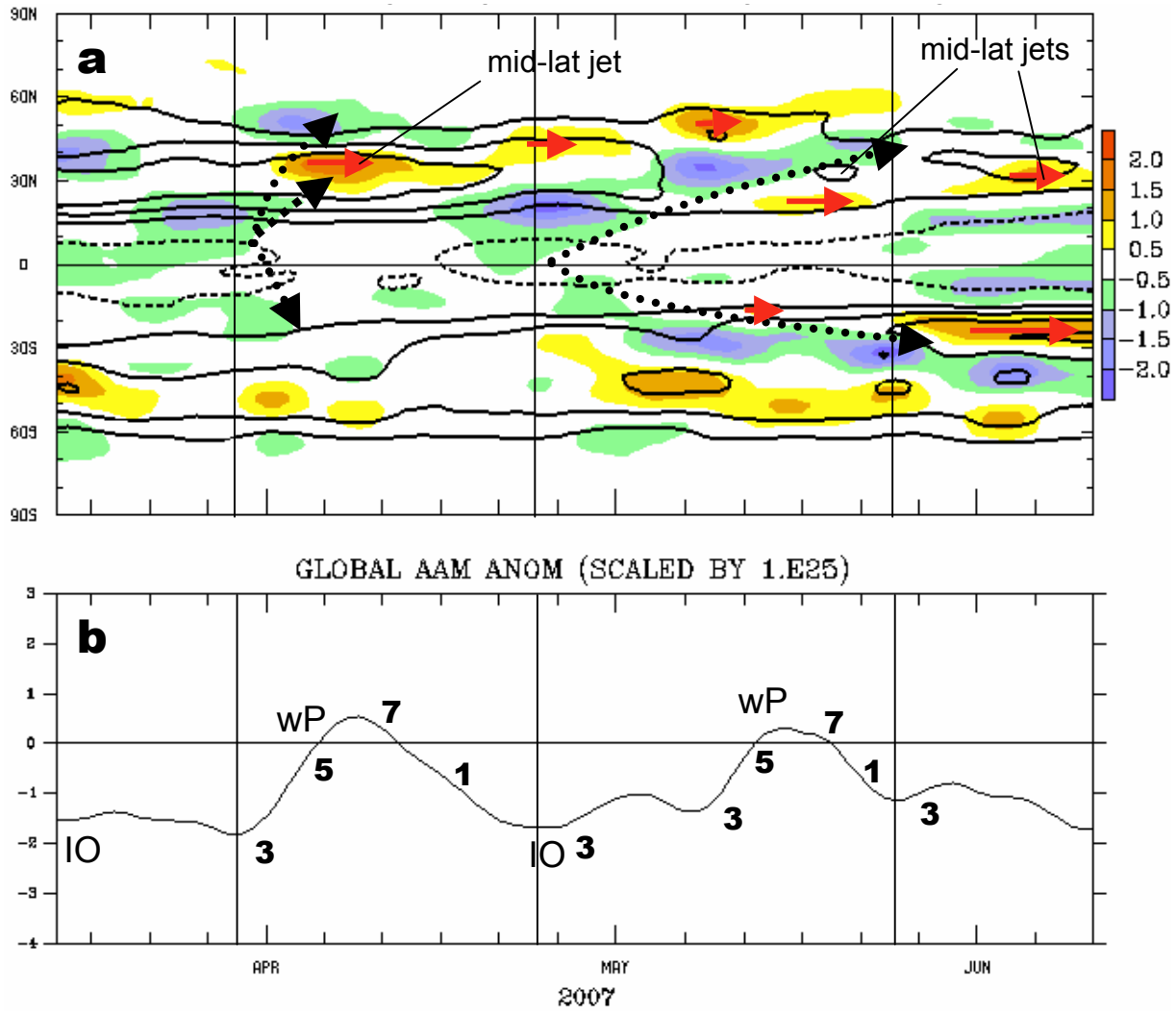

Fig. 7 a) The zonal relative AAM anomaly ($[\{m_r\}]_\varphi$) as a function of latitude and time for a 90-day period that includes the case study. The vertical lines denote the boundary of the orbits seen in Fig. 6. The contours show the total zonal AAM with a contour interval of 2.0×10^{24} kgm^{2}s^{-1} while the shading shows negative and positive anomalies with a shading interval of 0.5×10^{24} kgm^{2}s^{-1}. Annotations show the poleward movement of positive zonal AAM tendencies while the red arrows emphasize regions with westerly flow anomalies. The "mid-lat jet(s)" point to three periods of strong total and anomalous westerly flow between 20-40N. b) the global relative AAM anomaly (M_R), which is the meridional sum of a), is shown. Some GWO phases have been marked along the global time series, and the times when Indian Ocean (IO) or west Pacific (wP) convection was active.

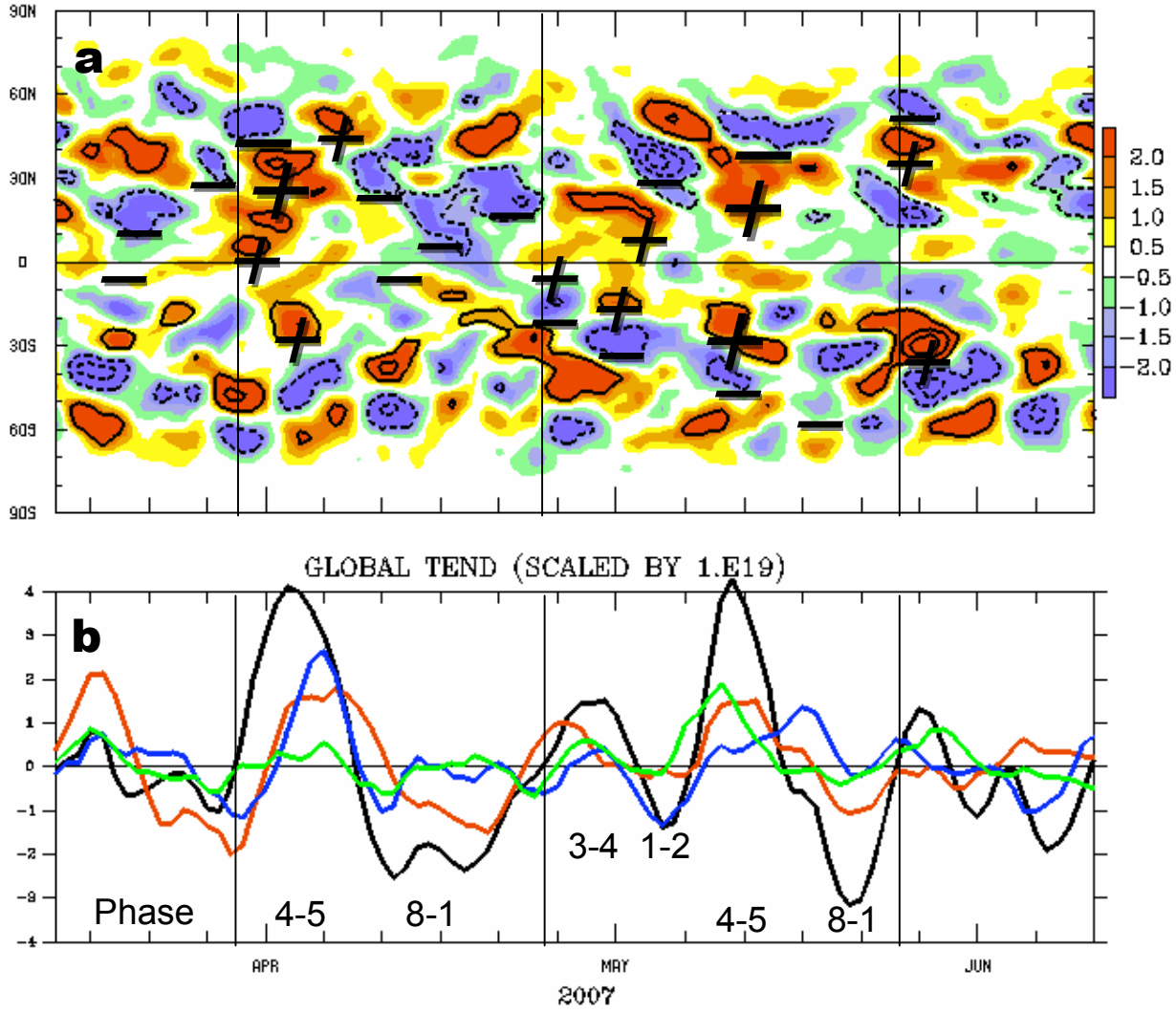

Fig. 8 a) Same as Fig. 7, except the relative AAM tendency ($[\{m_r\}]_\varphi$) is shown. The contour interval is 2.0×10^{18} kgm^2s^{-2} and the shading interval is 0.5×10^{18} kgm^2s^{-2}. The poleward movement of positive and negative tendency is highlighted with "+" and "-" symbols. b) the global relative AAM tendency (dM_R/dt) is shown by the black curve while the colored curves show the Asian mountain torque (red, see W03 for definition), the North American torque (blue) and the South American mountain torque (green). GWO phases are again marked on the bottom figure. The 8-1 phase evolution in late May was the basis for a week 2 forecast of a trough over the western USA. See text for further discussion.

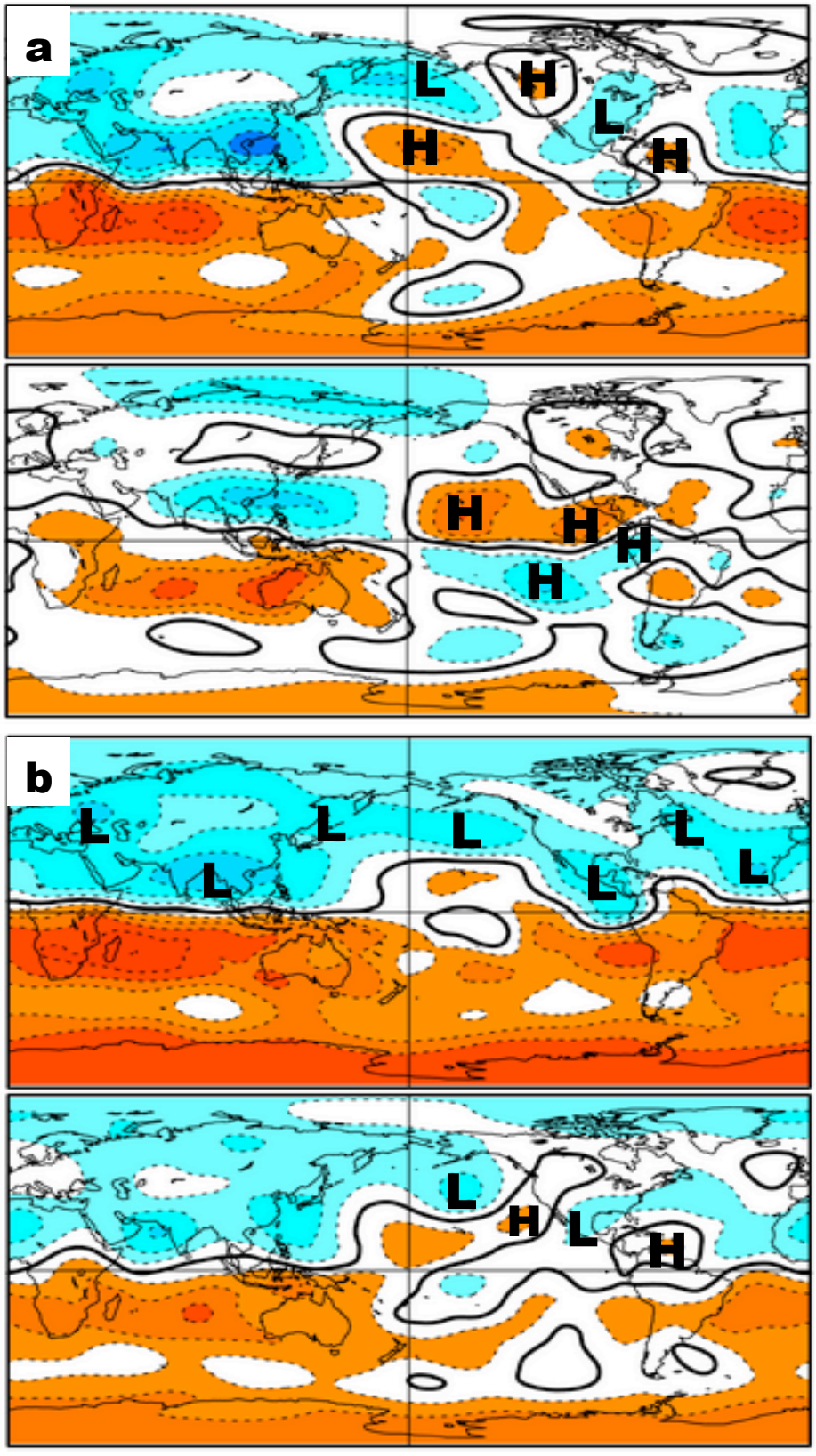

Fig. 9 A portion of the a) MJO and b) GWO life cycle of 250 hPa streamfunction anomaly during December-January-February is shown. The contour and color interval is 0.2σ where σ is the daily local standard deviation. The zero line is bold. See text for further discussion.